Current Biology 17, 1286–1297, August 7, 2007 ©2007 Elsevier Ltd All rights reserved DOI 10.1016/j.cub.2007.06.070

Article

Astral Signals Spatially Bias Cortical Myosin Recruitment to Break Symmetry and Promote Cytokinesis

Michael Werner,[1] Ed Munro,[2,*] and Michael Glotzer[1,*]
[1] Department of Molecular Genetics and Cell Biology
University of Chicago
920 East 58th Street
Chicago, Illinois 60637
[2] Center for Cell Dynamics
Friday Harbor Laboratories
University of Washington
620 University Road
Friday Harbor, Washington 98250

Summary

Background: After anaphase, the segregated chromosomes are sequestered by cytokinesis into two separate daughter cells by a cleavage furrow formed by the actomyosin-based contractile ring. The failure to properly position the contractile ring between the segregated chromosomes can result in aneuploidy. In both *C. elegans* embryos and human cells, the central spindle regulates division-plane positioning in parallel with a second pathway that involves astral microtubules.
Results: We combined genetic and pharmacological manipulations with live cell imaging to spatially separate the two division cues in a single cell. We demonstrate that the two pathways for furrow formation are mechanistically and genetically distinct. By following the distribution of green fluorescent protein (GFP)-tagged nonmuscle myosin, we have found that the astral pathway for furrow formation involves the negative regulation of cortical myosin recruitment. An asymmetrically positioned spindle induces the asymmetric cortical accumulation of myosin. This cortical myosin behaves as a coherent contractile network. If the cortical network is nonuniform over the cell, the cortical contractile elements coalesce into a single furrow. This coalescence requires interconnections among contractile elements.
Conclusions: We conclude that the two pathways of cleavage-furrow formation are mechanistically distinct. In particular, we conclude that the astral pathway for cleavage-furrow formation involves the negative regulation of myosin distribution by astral cues.

Introduction

Cell division in animal cells is mediated by an actomyosin-based contractile ring that forms at the site of the presumptive cleavage furrow and separates the two nascent daughter cells in a process called cytokinesis. If the two daughter cells are to inherit a complete copy of the genome, cytokinesis must be spatially and temporally coordinated with chromosome segregation. Spatial regulation of cytokinesis is also critical for asymmetric cell division because the cleavage furrow must be precisely positioned in order for the two daughter cells to receive appropriate dowries of cell fate determinants. Although it has been established that the mitotic spindle directs the positioning of the division plane, the underlying molecular mechanisms remain incompletely understood.

Positioning and assembly of the contractile ring are critical early steps in cytokinesis. The contractile ring contains large numbers of actin filaments and minifilaments of nonmuscle myosin. Contractile-ring assembly requires the small GTPase RhoA and its guanine nucleotide exchange factor, ECT-2, myosin regulatory light chain (rMLC), and myosin heavy chain (MHC, NMY-2). These proteins constitute a regulatory cascade required for the local activation of actomyosin-based contractility during cytokinesis (see [1] for review). At anaphase onset, the localized accumulation of an active form of the small GTPase RhoA prefigures contractile-ring assembly [2, 3]. RhoA regulates rMLC phosphorylation to promote myosin polymerization and contractile-ring assembly. RhoA also promotes formin-mediated actin polymerization in the cleavage furrow (see [4] for review). Myosin II motor molecules assemble into minifilaments that move actin filaments relative to one another to provide the driving force for constriction.

The position of the division plane is determined by the position of the spindle during anaphase. In several cell types, two parts of the spindle function redundantly to establish the division plane: the central spindle and the astral arrays of microtubules that surround the two spindle poles. The central spindle is composed of antiparallel microtubule bundles that lie between the spindle poles during anaphase. A core component of the central spindle is centralspindlin, a complex containing RhoGAP and kinesin subunits (CYK-4 and ZEN-4/MKLP1, respectively). In *C. elegans* embryos, the central spindle is dispensable for furrow initiation because depletion of either of its core components or of the microtubule-associated protein SPD-1 disrupts the central spindle but does not prevent cleavage-furrow ingression [5–8]. Conversely, cells of *Drosophila asterless* mutants are largely depleted of astral microtubules yet form cleavage furrows [9], suggesting that the central spindle is sufficient to direct cleavage-furrow formation. This apparent contradiction was resolved by genetic and laser-manipulation experiments that indicated that parallel pathways can act redundantly to induce furrow formation [10, 11]. Thus, the central spindle is usually dispensable for furrow formation in *C. elegans* embryos, but it nevertheless has furrow-inducing capacity. In the absence of a functional central spindle, the position of the division plane is determined by the position of the spindle, such that the furrow forms between the two asters [10, 11]. Although cleavage-furrow formation is usually directed by a bipolar spindle, cultured mammalian cells form furrows in the absence of a bipolar spindle

*Correspondence: munroem@uwashington.edu (E.M.), mglotzer@uchicago.edu (M.G.)

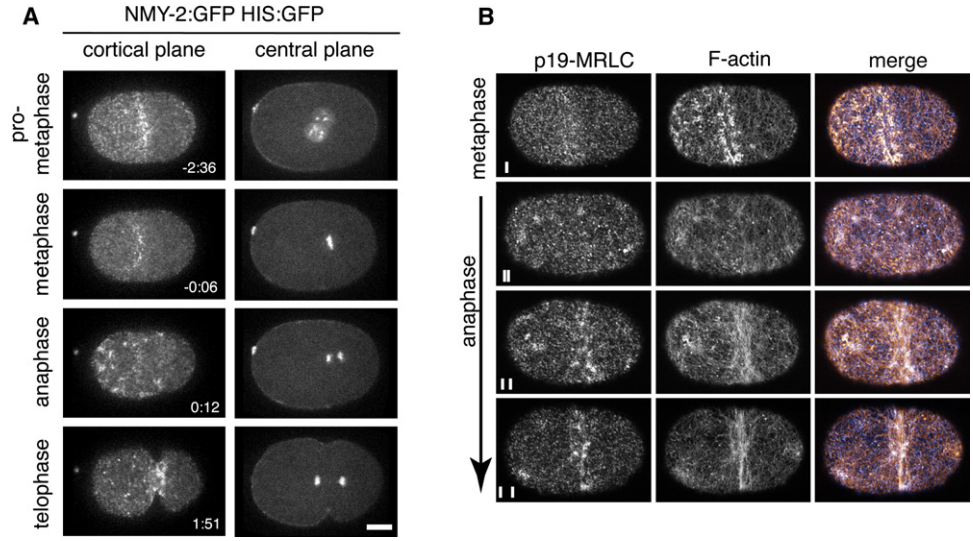

Figure 1. Cortical Myosin Undergoes Cell-Cycle-Regulated Changes in Its Localization

(A) A strain expressing both NMY-2:GFP and HIS:GFP was imaged during the first cell division.

(B) Spatial distribution of cortical F-actin and active myosin II during early stages of cytokinesis. Fixed whole-mount embryos stained with an antibody to serine-19-phosphorylated myosin regulatory light chain (p19-mRLC) (left) and stained with phalloidin to reveal filamentous actin and visualized by a single grazing plane using confocal microscopy. Vertical bars indicate the approximate separation of chromosomes in each embryo.

In all panels, anterior is to the left, time is relative to anaphase onset, and scale bars represent 10 μm.

[12]. In the more extreme case, cells largely depleted of microtubules exhibit dramatic albeit highly disorganized contractions for a limited time period after anaphase onset [13, 14]. Thus cortical contractility does not appear to require microtubules, but rather microtubule-based structures coordinate contractility so that it occurs at the appropriate site.

A molecular pathway has been defined that appears sufficient to explain how the central spindle induces furrow formation. HsCYK-4 has been shown to directly recruit the RhoGEF ECT2 [2, 15, 16]. This interaction is critical for RhoA activation and contractile-ring assembly. Furthermore, in human cells, HsCYK-4 is required for contractile-ring assembly, but its partner protein, MKLP1, is not, indicating that HsCYK-4 can promote RhoA activation without being localized to the central spindle [2]. Therefore, in human cells, as in *C. elegans* embryos, furrow formation does not strictly require the central spindle.

Whereas this molecular pathway can account for furrow induction by the central spindle, less information is available to explain the aster-regulated pathway [17]. To analyze how the central spindle-independent, astral, pathway can lead to the formation of a cleavage furrow, we monitored the cortical recruitment of green fluorescent protein (GFP)-tagged nonmuscle myosin (NMY-2) at high spatial and temporal resolution during the first cell division of the *C. elegans* embryo. We demonstrate that anaphase onset triggers the RhoA-dependent recruitment of cortical myosin. Using genetics or chemical treatments to misposition the mitotic spindle within the embryo, we demonstrate that the astral pathway functions by locally inhibiting myosin recruitment to the cell cortex. Subsequent coordinated reorganization of the anisotropic actomyosin network generates a contractile structure that drives furrowing.

Results

Dynamic Redistribution of Cortical Myosin upon Anaphase Onset in the Early *C. elegans* Embryo

To investigate the molecular mechanisms underlying the redundant pathways for cleavage-furrow positioning, we followed the distribution of GFP-tagged NMY-2 [18] before and during the initial stages of cytokinesis. In order to precisely time key transitions in myosin organization and dynamics relative to other cell-cycle events, we simultaneously visualized NMY-2:GFP and GFP-Histone (Figure 1A). During prophase, as the centrosomes and nuclei migrate toward the center of the zygote, the cortex is polarized, and small particles of myosin are enriched in the anterior portion of the embryo, forming a structure we will refer to as an anterior cap. This anterior cap persists until metaphase, when myosin largely dissociates from the cortex. During the first 30 s after anaphase onset, myosin reaccumulates on the cell cortex, primarily in bright foci. Hereafter, the term foci will refer to this population of myosin that accumulates upon anaphase onset. The initial recruitment of anaphase foci is broadly biased to the anterior two thirds of the embryo, with strongest accumulation in a broad equatorial band (centered midway between the spindle poles) and at the extreme anterior. During the next 60 s, myosin foci and smaller myosin-containing particles within the equatorial band move toward the center as a cleavage furrow forms and begins to ingress (Figure 1A, Movie S1 in the Supplemental Data available online). Similar distributions of myosin were observed in fixed specimens costained with an antibody specific for the serine-19-phosphorylated form of rMLC and with fluorescent phalloidin to label filamentous actin (F-actin) (Figure 1B). Interestingly, the foci of myosin colocalize with regions of high local F-actin density. The

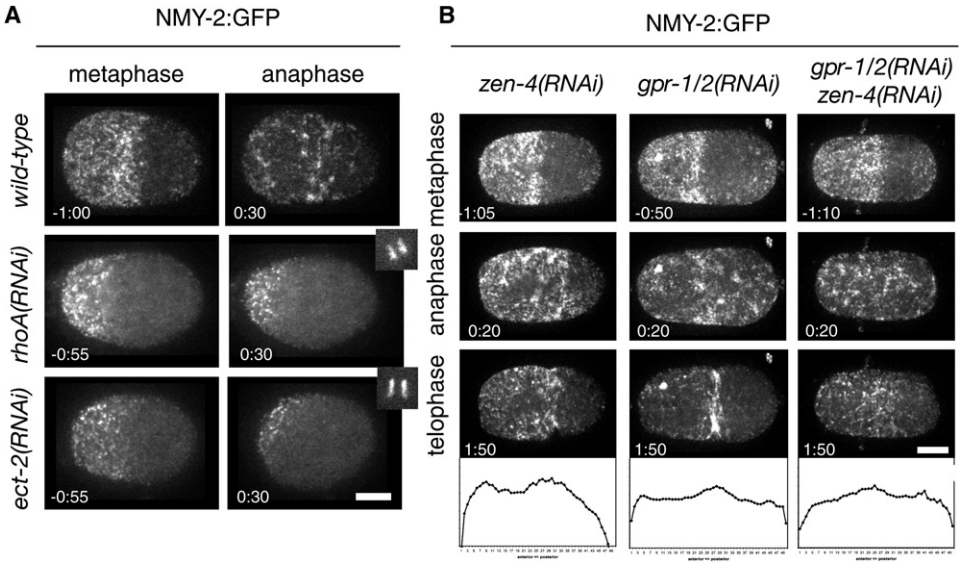

Figure 2. Cortical Myosin Accumulation upon Anaphase Onset Is Dependent on Active RhoA

(A) Formation of the anterior cap in prometaphase occurs in wild-type and *rhoA(RNAi)* or *ect-2(RNAi)* embryos, but depletion of these factors blocks cortical reaccumulation upon anaphase onset.

(B) Myosin accumulates at the anterior and equatorial cortex in *zen-4(RNAi)* embryos, and accumulates throughout the entire cortex in early anaphase in *gpr-1/2(RNAi)* and *zen-4(RNAi);gpr-1/2(RNAi)*. Also shown are normalized profiles of myosin distribution (averages of > 7 embryos) along the A/P axis at early anaphase.

accumulation of foci near the equator prior to furrow initiation correlates with the emergence of aligned circumferential filament bundles that connect neighboring foci.

To test whether the loss of cortical myosin in metaphase and the sudden accumulation of cortical myosin foci at anaphase onset are coordinated with cell-cycle progression, we delayed mitotic exit by depleting embryos of the proteasome regulatory subunit RPT-6. Control and RPT-6-depleted embryos required the same time to align their chromosomes on a metaphase plate after nuclear-envelope breakdown (NEBD), but the time from NEBD to anaphase onset is increased in RPT-6-depleted embryos ([19], McCarthy and Goldstein, personal communication). Myosin recruitment in these embryos was also delayed relative to NEBD, in precise correlation with the delay in anaphase onset (Figure S1A). We conclude that cortical recruitment of myosin requires the initiation of mitotic exit.

The Molecular Requirements for Cortical Myosin Recruitment

RhoA is a critical regulator of cytokinesis. RhoA depletion prevents furrow formation and inhibits cortical contractility and the formation of the pseudocleavage furrow [7, 20, 21], in part through myosin regulation [4]. We investigated how the depletion of RhoA affects myosin recruitment during cytokinesis. As shown previously, embryos severely depleted of RhoA lack an organized meshwork of cortical myosin during early interphase; loosely distributed small spots of myosin are observed, but the focal contractions that accompany polarization are absent. As in the wild-type, a cortical cap of smaller myosin-containing particles forms during prophase, although it is often smaller and displaced. The anterior cap starts to disappear on schedule during metaphase, but myosin remains at low levels throughout anaphase (Figure 2A, Figure S1B) instead of recruiting as intense foci to the anterior cortex and subsequently accumulating at the equatorial region. To assess whether this requires RhoA activation, we depleted the Rho guanine exchange factor (GEF) ECT-2. ECT2 depletion abrogates furrow formation in numerous cell types [2, 10, 22]. ECT-2 depletion prevented the cortical recruitment of myosin during early interphase and anaphase but did not abolish the anterior cap of myosin in prophase (Figure 2A, Figure S1B). Thus, significant recruitment of myosin to the cortex and myosin-driven contraction during anaphase require active RhoA.

Spatial and Functional Separation of Two Mechanisms for Furrow Ingression

Central spindle-dependent and -independent mechanisms act redundantly to regulate formation of the cleavage furrow [10, 11]. Embryos defective in either central spindle assembly (e.g., *zen-4(RNAi)*) or spindle elongation (e.g., *gpr-1/2(RNAi)*) form cleavage furrows, but embryos in which both spindle elongation and central spindle assembly are defective do not furrow. To determine why these embryos fail to furrow, we compared cortical distributions of NMY-2:GFP in *zen-4(RNAi)* (n = 13), *gpr-1/2(RNAi)* (n = 20), and *zen-4(RNAi)*; *gpr-1/2(RNAi)* (n = 9) embryos. During prophase and metaphase, all embryos exhibited wild-type myosin dynamics. At anaphase onset, in ZEN-4-depleted embryos, the initial pattern of anaphase myosin recruitment was indistinguishable from that of the wild-type; foci were enriched at the equator and in the anterior of the embryo. By contrast, in GPR-1/2-depleted embryos, the broad anterior bias in the initial recruitment of cortical myosin foci was lost, but the slight enrichment at the equator was

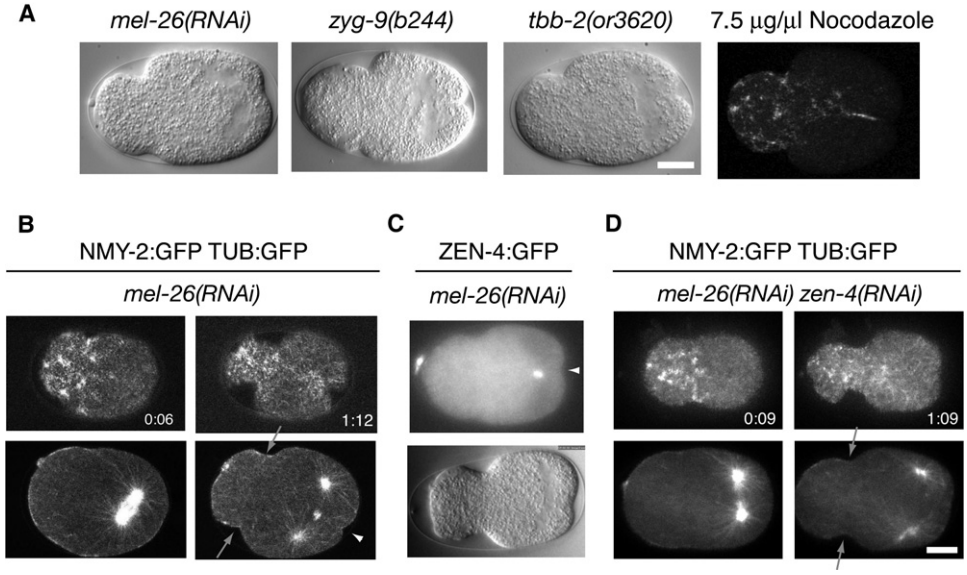

Figure 3. Genetic and Spatial Separation of Two Redundant Pathways for Furrow Formation within One Embryo

(A) Differential-interference contrast (DIC) images of embryos with perturbed microtubule stability form a small posterior spindle and two cleavage furrows.

(B) Embryos with a posterior spindle accumulate myosin in the anterior and form an anterior furrow (arrow). A second, central spindle-dependent furrow forms in the posterior (arrowhead). NMY-2:GFP and TUB:GFP were visualized in the same embryo. Myosin can be observed in cortical planes (top), whereas tubulin is visualized in the central plane of the embryo (bottom). Representative images at the indicated times after anaphase onset are shown.

(C) ZEN-4:GFP localizes to the central spindle in embryos with posterior spindles.

(D) The anterior furrow (arrows) but not the posterior furrow forms when central spindle assembly is prevented.

not. In embryos defective in both central spindle assembly and spindle elongation, myosin foci were recruited to the cortex uniformly; however, there was no equatorial bias, and in this case, furrow formation was not observed (Figure 2B). Because cortical recruitment of intense myosin foci requires active RhoA, we conclude that the failure of these embryos to furrow is not because of a failure to activate RhoA. Moreover, the initial recruitment of cortical myosin is central spindle independent. We measured average intensity values along the A/P axis at anaphase onset. These data confirm that myosin is uniform in GPR-1/2; ZEN-4-depleted embryos (Figure 2B). Instead, the comparison between *zen-4(RNAi)* embryos and *zen-4(RNAi)*; *gpr1/2(RNAi)* embryos suggests that the asymmetric accumulation of myosin requires asymmetric spindle positioning.

To further characterize the mechanism of furrow formation, we sought to spatially separate these two pathways. Chemical perturbations of the microtubule cytoskeleton in the early embryo cause the misplacement of the spindle to the posterior and the subsequent formation of two cleavage furrows [23]. The posterior furrow initiates near the misplaced mitotic spindle, bisecting it. The anterior furrow forms at a distance from the mitotic spindle (Figure 3A). Multiple perturbations elicit the same effect: microtubule destabilization with nocodazole, a conditional allele of β-tubulin, *tbb-2(or3620ts)*, depletion or mutation of the microtubule-associated protein (MAP) ZYG-9, or mutations or depletion of MEL-26. To assess how myosin distribution during anaphase is altered in response to perturbed spindle location and geometry, we simultaneously monitored the distribution of cortical myosin and cytoplasmic microtubules by using confocal microscopy. Until anaphase, embryos with posterior spindles exhibited myosin dynamics indistinguishable from those of the wild-type. The initial appearance of myosin foci was biased to the anterior, and there was no preferential accumulation at the equator (Figure 3B). A furrow subsequently formed at the edge of the domain enriched in myosin foci. After the recruitment of anterior foci, cortical myosin accumulated in the posterior cortex between the spindle poles, forming a second furrow (Figure 3B, Movie S2). Cortical myosin accumulation and formation of both furrows required ECT-2 (data not shown). Thus, two furrows can form in a single embryo with a posterior spindle, and these furrows have distinct positions relative to the spindle and display distinct modes of myosin recruitment and reorganization.

Next, we examined whether these two furrows are differentially dependent on the central spindle. In MEL-26-depleted embryos, ZEN-4:GFP localizes to the spindle midzone during anaphase, confirming that a central spindle forms (Figure 3C). We depleted MEL-26 by RNAi either alone or in combination with *zen-4(RNAi)*. During anaphase, in both *mel-26(RNAi)* and *mel-26(RNAi)*; *zen-4(RNAi)* embryos, the mitotic spindle formed in the posterior of the embryo and, upon anaphase onset, cortical myosin accumulated and reorganized to create an anterior furrow. Thus, as shown above for myosin recruitment and furrow initiation in the wild-type, the anterior mode of furrow formation is independent of the central spindle. By contrast, in *zen-4(RNAi)*; *mel-26(RNAi)* embryos, myosin did not accumulate in the posterior cortex over the spindle, and no posterior furrow appeared (n = 8) (Figure 3D). Identical results

were obtained when we produced posterior spindles by other methods or when *zen-4(or153ts)* was used to inhibit central spindle assembly (n = 6). Thus, central spindle-dependent and -independent mechanisms of patterning cortical myosin recruitment and furrow initiation can be analyzed in the same embryo. Furthermore, the anterior furrow and the central spindle-independent furrow have similar genetic requirements, both positive and negative, and display similar patterns of myosin accumulation. In contrast, the anterior and posterior furrows can be distinguished by these criteria.

Spindle Positioning Spatially Biases Myosin Accumulation through Local Inhibition, but the Total Accumulation Is Constant

To gain insight into the patterning of Rho-dependent myosin recruitment in anaphase, we quantitatively compared the accumulation of cortical myosin in control embryos and embryos with posterior spindles. Every 2.5 s, we acquired five confocal sections, generated projections, and created kymographs from line scans along the A/P axis. In embryos with posterior spindles, as in wild-type embryos, foci appeared within 5 s of anaphase onset. In the anterior half of the embryo, the size, intensity, and local spacing of foci were the same as they were in the wild-type. By contrast, only small foci accumulated in the posterior cortex, as in wild-type embryos (Figures 4A and 4B). Thus, the initial recruitment of myosin at anaphase is inhibited in the neighborhood of the posterior mitotic spindle, probably because of a failure to recruit myosin, rather than its recruitment and subsequent displacement.

We quantified the distribution of these foci, because they first appear after the onset of anaphase. In wild-type embryos, the initial anaphase accumulation of myosin foci is weakly biased in favor of the anterior, with many embryos showing an early peak of accumulation at the equator and the extreme anterior, with minima between these peaks and the extreme posterior (Figure 4D). Strikingly, embryos with a posterior-localized spindle (e.g., *mel-26(RNAi)*) exhibit a stronger bias in the accumulation of myosin foci and lack an equatorial peak. This anterior bias is induced by the asymmetrically positioned spindle because it was suppressed when the spindle was symmetrically positioned because of the depletion of PAR-3 or PAR-2 (Figure 4D and data not shown, respectively).

We next analyzed the total accumulation of myosin at anaphase onset in embryos of various genotypes to determine whether the local inhibition of myosin recruitment near the spindle causes an overall reduction in total myosin accumulation or a shift in myosin accumulation away from the spindle. Total cortical myosin accumulation was not significantly affected by the position of the spindle (Figure 4C).

Although myosin is polarized prior to metaphase and occupies the same region of the embryo as in anaphase, these patterns are independent. Kymograph analysis shows that distribution of the anaphase foci does not directly correlate with the position or extent of the anterior cap (Figures 4A and 4B). In addition, *zen-4(or153); gpr-1/2(RNAi)* embryos exhibit an anterior cap of myosin in prophase, but in anaphase, myosin is uniformly distributed to the entire cell cortex (Figure 2C).

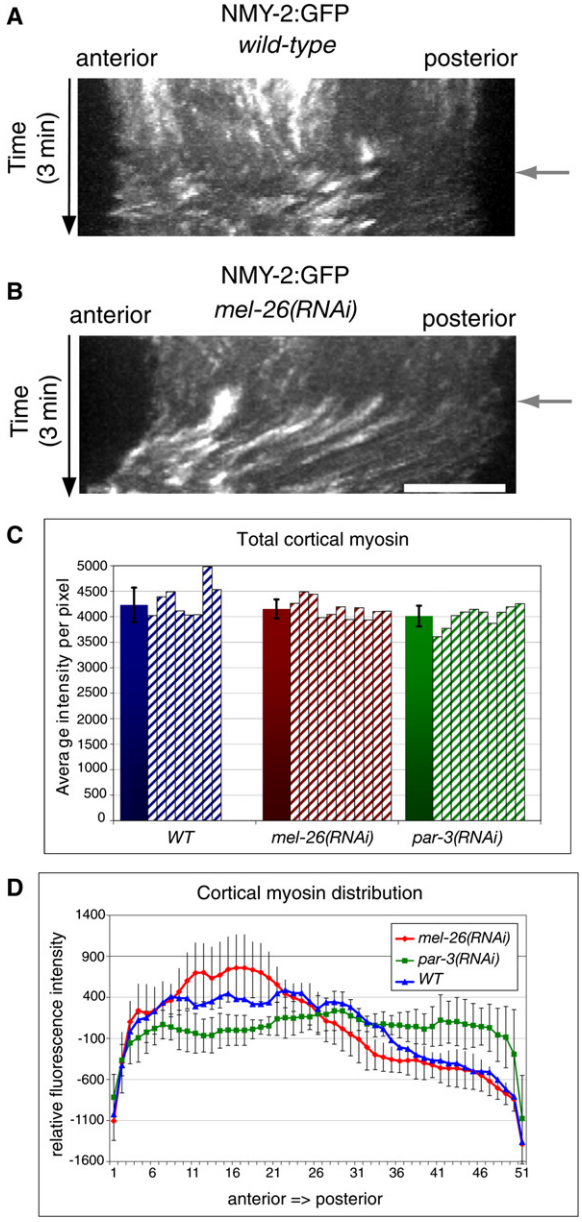

Figure 4. The Position of the Mitotic Spindle Controls Cortical Myosin Distribution

(A and B) Kymographs of cortical myosin distribution in wild-type embryos (A) and embryos with a posterior spindle (B). Anaphase onset (gray arrow) was determined by the appearance of cortical myosin foci.

(C) The cortical myosin distribution after anaphase onset was determined by the measurement of the average cortical intensity of NMY-2:GFP (± the standard deviation [SD]) over the first 20 s after anaphase onset, representing eight time points. Measurements for wild-type embryos (blue), embryos with posterior-positioned mitotic spindles, *mel-26(RNAi)* (red), and embryos with symmetrically positioned spindles, *par-3(RNAi)* (green) are shown. The data from at least eight individual recordings were normalized for the length of the embryo.

(D) Average total cortical myosin after anaphase onset was measured during the first 20 s after anaphase onset. The graph represents average total intensity per pixel values (solid bars) (± the SD) for at least eight individual recordings, as well as the values for the individual recordings (stripes).

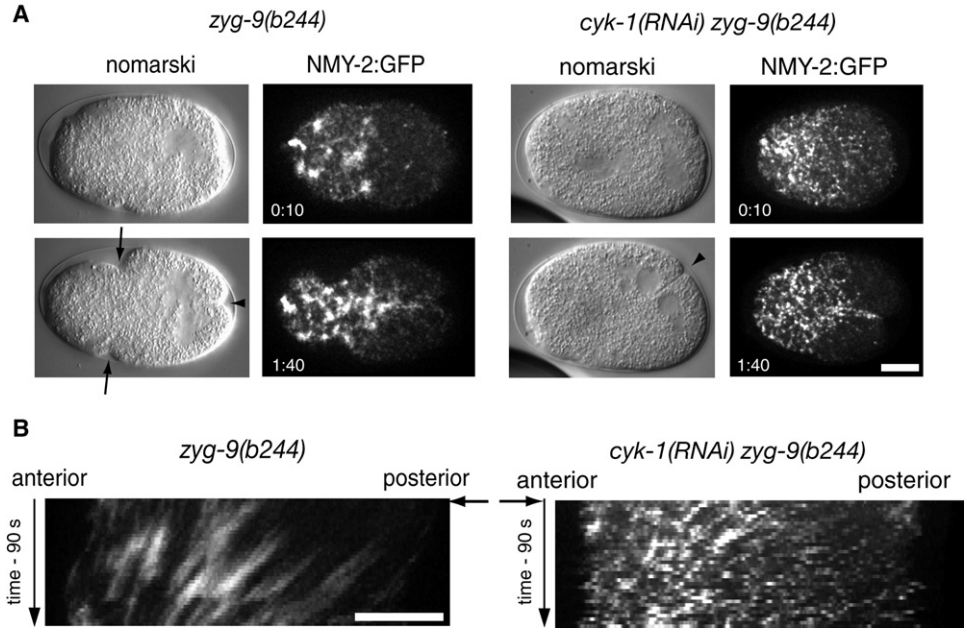

Figure 5. Coordinated Cortical Myosin Contractions Are Required for the Formation of the Anterior Furrow

Nomarski images and images from embryos expressing NMY-2:GFP after anaphase onset and in telophase. Embryos with a posterior spindle but unperturbed cortical actomyosin (*zyg-9(b244)*) show anterior myosin localization and formation of an anterior and a posterior furrow (A), whereas embryos with perturbed cortical actomyosin (*zyg-9(b244); cyk-1(RNAi)*) only form a posterior furrow, although myosin still localizes to the anterior. Nomarski and NMY:2:GFP images are representative images from different recordings. Kymographs from corresponding NMY-2:GFP recordings are shown (B). Anaphase onset is indicated by a black arrow.

The Anterior Furrow Emerges from the Coherence of Contractile Elements in the Cortex

After the initial, polarized recruitment of myosin in embryos with posterior spindles, cortical myosin foci move collectively toward one another and toward the anterior, revealing a large-scale contraction away from the zone of myosin depletion at the posterior (Figure 4B). The anterior furrow then forms at the edge of the domain enriched in myosin foci. Because this appears to involve coordinated behavior of myosin foci, we investigated how the anterior furrow responds to perturbation of the actomyosin network. The formin-homology-domain-containing protein CYK-1 is required for normal F-actin assembly in the early embryo and furrow initiation at cytokinesis. Although CYK-1 is required for furrow formation, maternal-effect lethal mutations and RNAi-mediated partial depletion of CYK-1 allow cleavage-furrow ingression [24]. We confirmed that *cyk-1(RNAi)* embryos reproducibly form furrows during a 5 hr window of RNAi depletion (n = 9). Furrow formation in embryos partially depleted of formin activity requires the central spindle, because *cyk-1(or36); zen-4(or153ts)* double-mutant embryos do not furrow [25]. Likewise, we find that *zen-4(or153ts)*; *cyk-1(RNAi)* embryos consistently fail to furrow (n = 8). Next, we examined whether the anterior and posterior furrows in *zyg-9(b244)* mutant embryos are differentially sensitive to partial formin depletion. CYK-1 was partially depleted in *zyg-9(b244)* mutant embryos with the above conditions. All *zyg-9(b244)*; *cyk-1(RNAi)* embryos failed to form an anterior furrow, yet a majority of these same embryos (63%) formed a deeply ingressing posterior furrow (n = 11) (Figure 5A). Thus, the anterior and posterior furrows are differentially sensitive to CYK-1 depletion. Moreover, this extends the genetic similarities of the anterior furrow and the equatorial furrow in embryos lacking a central spindle.

To determine why the anterior cleavage furrow fails to form under these conditions, we examined NMY-2:GFP in *cyk-1(RNAi)*; *zyg-9(b244)* embryos. In these embryos, as in the *zyg-9* single mutant, NMY-2 accumulates at anaphase onset with similar kinetics and a strong anterior bias. However, in *cyk-1(RNAi)*; *zyg-9(b244)* embryos, as anaphase proceeds, the myosin foci are smaller and more dispersed. Instead of the coherent flows of myosin seen in *zyg-9(b244)* embryos, we observed short-range flows in a variety of directions (Figure 5B). A single furrow failed to form at the edge of the anterior myosin-rich domain; instead, we observed small cortical ruffles throughout the anterior (Movies S2 and S3). To characterize the defect further, we quantified the relative movements of individual pairs of myosin foci (Figure S2B). In wild-type embryos and embryos with posterior spindles, pairs of foci most often move toward one another at rates less than 4 μm/min. However, when CYK-1 is depleted, particle movements are greatly exaggerated, and pairs of foci frequently move away from each other at rates that often exceed 4 μm/min. Together these data suggest that when CYK-1 is limiting, mechanical coupling of neighboring contractile elements is diminished or lost; they suggest, furthermore, that this mechanical coupling is necessary to produce a globally coordinated contraction and to resolve a single deeply ingressing furrow instead of many weak and transient invaginations. Thus, the posterior spindle promotes the biased accumulation of contractile elements that then assemble into

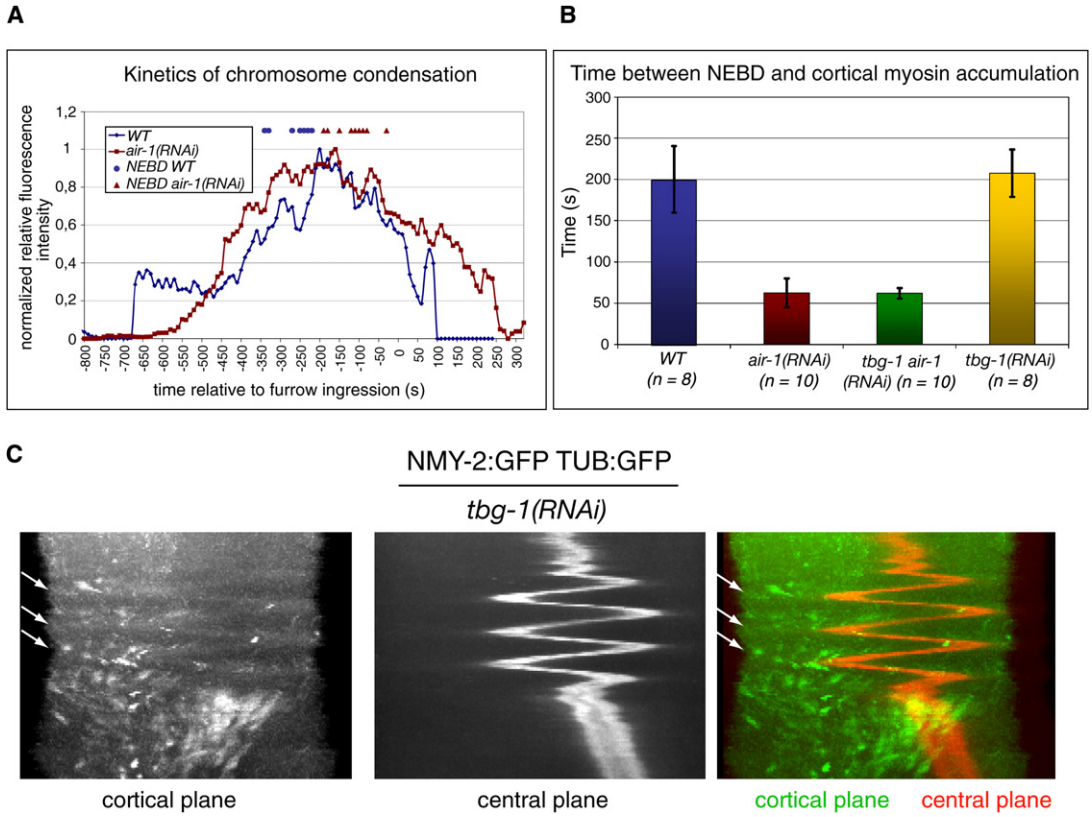

Figure 6. Spindle Oscillations Inhibit Myosin Accumulation in Embryos Depleted of γ-Tubulin

(A) Timing of chromosome condensation relative to furrow ingression in wild-type and *air-1(RNAi)* embryos. The measurements shown are averages for at least eight individual recordings of embryos expressing both NMY-2:GFP and HIS:GFP. The time of NEBD of each individual recording is indicated for wild-type ("•") and *air-1(RNAi)* ("▲") embryos.

(B) Average time (± the SD) of cortical myosin accumulation relative to NEBD.

(C) Overlay of kymographs taken along the same line of a maximum projection of five cortical planes (green) and one central plane (red) of a movie of an embryo expressing NMY-2:GFP and TUB:GFP. Arrows indicate a subset of foci that accumulate when the spindle is at a distance and dissociate as it returns.

a globally coupled, contractile network that creates a single furrow as an emergent behavior.

Do γ-Tubulin-Nucleated Microtubules Positively Regulate Furrowing?

In contrast to the results presented here, it has recently been proposed that γ-tubulin nucleated microtubules promote the initial accumulation of contractile-ring components [21]. The data that led to this proposal are that (1) AIR-1-depleted embryos form a γ-tubulin-dependent precocious furrow shortly after NEBD and that (2) furrowing often fails in γ-tubulin-depleted embryos.

The conclusion that furrows form precociously in AIR-1-depleted embryos was based on a comparison of the timing of furrow initiation relative to NEBD. We confirmed the basic finding, measuring a delay between NEBD and furrow initiation of ~2 min in AIR-1-depleted embryos, as compared to ~4.5 min in wild-type embryos (116 ± 47 s and 265 ± 45 s, respectively). However, we and others have observed enhanced chromosome condensation at NEBD in AIR-1-depleted embryos as compared to wild-type embryos [26]. We therefore quantified the timing of chromosome condensation, NEBD, and the onset of furrowing in wild-type and AIR-1-depleted embryos and found no significant difference in the interval between chromosome condensation and furrow formation (Figure 6A). However, in wild-type embryos, NEBD was roughly coincident with half-maximal chromosome condensation, whereas in AIR-1-depleted embryos, NEBD occurred ~4 min after half-maximal chromosome condensation (0 ± 30 s and 240 ± 90 s, respectively) (Figure 6A). We conclude that AIR-1 depletion results in the delay of NEBD, and similar conclusions were recently published [27, 28]. Thus precocious furrowing does not occur in AIR-1-depleted embryos.

We next investigated whether γ-tubulin regulates the timing of anaphase recruitment of cortical myosin. We assayed NEBD and cortical myosin recruitment in wild-type, *air-1(RNAi)*, *tbg-1(RNAi)*, and *tbg-1(RNAi); air-1(RNAi)* embryos. The time interval between NEBD and cortical myosin accumulation at anaphase was ~3.5 min in both wild-type and *tbg-1(RNAi)* embryos (Figure 6B). In contrast, this time interval was only ~1 min in both *air-1(RNAi)* and *tbg-1(RNAi); air-1(RNAi)* embryos (Figure 6B). Thus, γ-tubulin does not regulate the onset of cortical myosin accumulation in anaphase.

Although myosin recruitment occurs on schedule in γ-tubulin-depleted embryos, furrow formation is

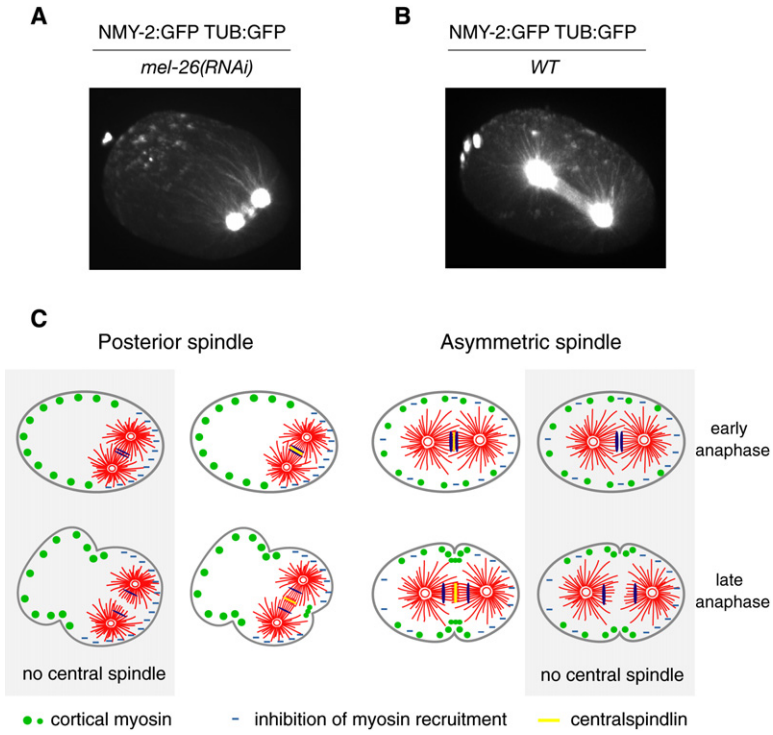

Figure 7. The Relative Positions of Myosin and Tubulin in Wild-Type Embryos and Embryos with Posterior Spindles

(A and B) 3D reconstructions of *mel-26(RNAi)* (A) and wild-type (B) embryos expressing NMY-2:GFP and TUB:GFP are shown shortly after anaphase onset, demonstrating reduced myosin accumulation in regions of high microtubule density.

(C) A model describing how the central spindle-dependent and central spindle-independent pathways regulate myosin localization and cooperate in furrow formation (see text for details).

frequently blocked in these embryos. One interpretation of these data is that γ-tubulin nucleated microtubules promote the recruitment of contractile-ring components, as suggested [21]. If this recruitment occurs and is independent of the central spindle as proposed, posterior spindles like those in *mel-26(RNAi)*; *zen-4(RNAi)* embryos would be predicted to induce a posterior furrow adjacent to the source of the positive signal. However, such furrows do not form (Figure 3D); rather, myosin is enriched exclusively in the anterior, and only an anterior furrow forms. To examine the requirement for γ-tubulin more closely, we simultaneously visualized the distribution of NMY-2 and microtubules in γ-tubulin-depleted embryos and discovered a remarkable phenotype. γ-tubulin depletion results in a monopolar spindle that undergoes rapid oscillations along the A/P axis, beginning shortly after anaphase onset (Figure 6C). Each oscillation covered 20–25 μm and required 20–30 s; the spindle moved at equal rates in each direction. As the spindle oscillated, cortical myosin transiently accumulated distal to the position of the spindle. As the spindle approached the newly recruited cortical myosin, it was displaced. Once the oscillations ceased, the monopolar spindle remained in the vicinity of the posterior pole of the embryo and furrow formation occurred in a fraction of the embryos. This furrow appeared to arise from a pool of myosin that accumulates in the anterior cortex, distal to the final position of the spindle. These data emphasize that high microtubule density inhibits myosin accumulation and that microtubules can reduce the cortical residence time of myosin foci.

4D Visualization of Myosin Dynamics

To further understand the relationship between the distribution of microtubules and the recruitment of cortical myosin, we collected high resolution Z series through the top half of embryos expressing GFP-tubulin and GFP-NMY2 during a short time interval surrounding furrow formation. These data sets were reconstructed into 4D images. Three-dimensional reconstructions of MEL-26-depleted embryos highlight the peripheral accumulation of myosin forming a cortical shell (Figure 7A, Movies S4 and S5). These images permit the visualization of the extent of the spindle and reveal that the bright foci of myosin are excluded from the portion of the cortex that is directly contacted by spindle microtubules. Analogous reconstructions of wild-type embryos demonstrate that cortical myosin recruitment is strongly inhibited in the vicinity of the posterior centrosome (Figure 7B, Movie S6). The inhibition was somewhat less striking and penetrant over the anterior centrosome. Most foci do not appear to specifically interact with astral microtubules. In a brief interval, ~20 s, the foci converge into an incomplete ring in the spindle midplane. The cortex begins to contract locally even before the ring is complete. Microtubule bundles are deformed as the furrow ingresses, ultimately forming the midbody, which sets the stage for cell separation.

Discussion

Here we have presented an analysis of the mechanism of cleavage-furrow positioning in the early *C. elegans* embryo on the basis of high-temporal- and high-spatial-resolution microscopy. Previous studies established that central spindle-dependent and central spindle-independent mechanisms are each sufficient to direct cleavage-furrow formation [10, 11]. Here, we have focused primarily on the aster-mediated pathway for furrow initiation. Our analysis points to a two-step mechanism for aster-mediated furrowing: First, a signal associated with astral microtubules locally inhibits

cortical myosin recruitment at anaphase onset, biasing myosin accumulation. Subsequently, these contractile elements coordinately contract to form a single cleavage furrow.

Probing Cytokinesis via Spindle Displacement and Manipulation

We have used genetic and pharmacological perturbations to displace the spindle within the embryo, in order to study the properties of the two furrow-inducing signals at the same time in the same embryo. Many insights into cytokinesis have been gleaned through spindle manipulations. For example, micromanipulation experiments established that the mitotic spindle controls cleavage-furrow positioning and ingression [29, 30]. Likewise, pharmacological inhibition of centrosome separation revealed that a monoaster is sufficient to direct cleavage-furrow formation [12]. Here, we used multiple methods to reduce spindle size and allowed the endogenous pathway for asymmetric spindle positioning to reposition the spindle in the posterior. These perturbations consistently resulted in two distinct furrows in a single embryo (Figure 7C). The posterior furrow forms in close apposition to the central spindle and requires the centralspindlin component ZEN-4; it reflects the central spindle-dependent pathway. The following criteria indicate that the anterior furrow reflects the central spindle-independent (astral-induced) furrow. Like the authentic cleavage furrow, anterior furrow formation involves the rapid appearance, and coordinated contraction, of myosin foci. These foci are highly similar in size, spacing, and timing of their appearance to those associated with furrow formation in wild-type embryos. The anterior furrow, like the furrow that forms in the embryos lacking a central spindle, is sensitive to the partial depletion of the formin CYK-1. Finally, like an unperturbed cleavage furrow, the anterior furrow requires RhoA and its RhoGEF, ECT-2.

Nonuniform Accumulation of Cortical Myosin and Its Coordinated Contraction Results in Furrow Formation

In all of the embryos we examined, with the exception of embryos depleted of RhoA and ECT-2, myosin II accumulates in foci within seconds of anaphase onset. Delaying anaphase onset correspondingly delays their appearance. In contrast, the kinetics of appearance of these foci are independent of spindle size and position and the presence or absence of a central spindle. In particular, in embryos doubly compromised for both ZEN-4 and GPR-1/2, foci appear with normal timing over the entire cortex, indicating that myosin can bind to the entire cortex upon exit from mitosis. Our data strongly suggest that the mitotic spindle patterns the accumulation of myosin foci by locally inhibiting their recruitment (Figure 7C).

Soon after their appearance during anaphase, in both wild-type embryos and embryos with posterior spindles, myosin foci move toward one another and toward regions of the embryo that are enriched in myosin. In both situations, myosin foci move in a similar pattern and at similar speeds and respond similarly to depletion of CYK-1 (Figure 5C, Figure S2B). Because previous work has shown that the movement of foci during pseudocleavage is driven by myosin-mediated contraction [18], the movements that occur during anaphase are probably also driven by myosin motor activity. Such movements are expected if contractile forces pulled each focus toward each of its neighbors. These foci might be functionally related to the nodes of contractile proteins that coalesce into the cleavage furrow in *S. pombe* [31]. The mechanical coupling between neighboring foci is probably mediated by the prominent bundles of F-actin that connect myosin foci. In embryos with a posterior spindle, the biased accumulation of myosin results in a furrow positioned near the border between regions of high and low myosin accumulation. Formation of this furrow is independent of the central spindle, and we do not detect centralspindlin components associating with it (data not shown). Furthermore, the partial depletion of CYK-1 prevents these foci from coalescing and concentrating in the anterior of the embryo and inhibits anterior furrow formation, but it does not significantly affect the initial asymmetry in myosin recruitment. Thus, the formation of the anterior furrow involves two distinct steps: Local inhibition produces biased accumulation of a cortical actomyosin network at anaphase onset; then the coordinated contraction of the network enhances this bias and promotes the production of a single coherent furrow.

Although the inhibition of myosin recruitment follows the distribution of astral microtubules, we do not yet know whether microtubules themselves mediate the inhibition or whether microtubules shape the distribution of another factor that is directly responsible for the inhibitory effect. The DEP-domain-containing protein, LET-99, has recently been suggested to be a specific regulator of the astral pathway [17]. We examined whether LET-99 is required for furrow formation in embryos with posterior spindles and found that depletion of LET-99 delays the appearance of the anterior furrow in *tbb-2(or3620ts)* embryos and reduces the extent of its ingression. However, anterior furrow formation was not abolished (n = 12, *let-99(RNAi); tbb-2(or3620ts)*, and n = 6, *let-99(RNAi); zyg-9(b244)*). The depletion of LET-99 in *tbb-2(or3620ts)* embryos did not dramatically affect the recruitment of myosin foci upon anaphase onset, but as the cell cycle proceeded, the cortical residence time of myosin foci was reduced and the anterior, myosin-enriched zone contracted farther toward the anterior pole (Movie S7, Figure S3). Thus, LET-99 appears to modulate actomyosin-based cortical contractility. The absolute requirement for LET-99 in embryos lacking a spindle midzone probably reflects its dual roles in regulating cortical components and its ability to modulate spindle positioning.

The myosin dynamics we observe during cytokinesis are similar to those observed during polarity establishment in the *C. elegans* zygote [18]. Initially, myosin-rich foci are distributed throughout the cortex. The sperm centrosome breaks cortical symmetry by inhibiting focus formation near the future posterior pole. The remaining meshwork contracts toward the anterior pole, and the pseudocleavage furrow transiently forms at the edge of the myosin-rich domain. Movements of myosin foci measured during pseudocleavage are quantitatively similar to those we observed during anaphase (Figures S2A and S2B), and the partial depletion of CYK-1 affects

these two processes similarly. However, embryo polarization is triggered by a microtubule-independent cue from the centrosome [32, 33]. Although different cues bias actomyosin contractility during these processes, the actomyosin dynamics that govern the response to these cues appear similar.

The posterior furrow forms near the central spindle in a cortical region otherwise depleted of cortical myosin. The central spindle could act positively to locally recruit an activating factor, such as ECT2, or by locally relieving the inhibitory activity of microtubules. At this juncture, we favor the former possibility because the central spindle can recruit the RhoGEF ECT2 in other organisms [2, 16]. Interestingly, this furrow can form in embryos with reduced CYK-1. This suggests that posterior furrow formation does not require long-range coordination between contractile elements but rather the local accumulation of myosin.

The Role of γ-Tubulin in Cleavage-Furrow Positioning

A previous study suggested that γ-tubulin-nucleated microtubules positively regulate furrow formation [21] because embryos depleted of γ-tubulin were furrowing defective and failed to accumulate the contractile-ring components RHO-1 and F-actin. We propose that in γ-tubulin, embryos fail to furrow for two reasons. First, rapid oscillations of the monoaster delays the stable accumulation of myosin by displacing myosin from cortical regions in close proximity to the monoaster. Second, γ-tubulin depletion sharply reduces microtubule number [34]. Modeling of a microtubule array in a closed system predicts that simply reducing microtubule nucleation permits more microtubules to approach the cell cortex because of reduced competition for tubulin dimers [35]. Thus, γ-tubulin depletion could generate a centrally located monoaster that prevents the biased accumulation of myosin.

Models for Cleavage-Furrow Positioning

Cells depleted of most microtubules undergo dramatic and disorganized cortical contractions for a defined time window after anaphase onset [13, 14], suggesting that microtubules can inhibit cortical contractility. Extending this finding, we had proposed that the two pathways that regulate cytokinesis might act through a common mechanism that generates a local minimum of microtubule density at the cell equator [36]. Subsequent work has indicated that concentration of the RhoA GEF, ECT2, to the central spindle promotes RhoA activation in a narrow zone overlying the central spindle [2, 15, 37]. By directly visualizing the distribution of microtubules and myosin II in live embryos, we have shown that cortical accumulation of this major contractile-ring component is negatively regulated by microtubules that emanate from the spindle. This behavior is conceptually similar to the astral-relaxation pathway [38]. Thus, cleavage-furrow formation in the early *C. elegans* embryo is triggered by a combination of positive and negative pathways. Furthermore, both pathways appear to regulate cytokinesis in other animal cells [2].

The negative regulation of cortical contractility by microtubules might not be limited to cytokinesis. Rearrangements of microtubules precede the cortical contractility that induces nuclear migration in neurons [39, 40]. Similarly, in cultured cells, microtubules suppress contractility [41, 42]. Finally, although the migration and polarization of fibroblasts ordinarily requires microtubules, fibroblasts lacking microtubules can be induced to migrate by the local application of myosin inhibitors [43]. Thus, the local modulation of cortical contractility is of general biological importance.

Experimental Procedures

Strains and Alleles

The following strains and alleles were used in this study: Bristol N2 (wild-type), *zen-4(or153ts)* IV, *xsEx6[zen-4:GFP rol-6]*, *zyg-9(b244)*, *tbb-2(or3620ts)*, *zuIs45* [NMY-2:GFP] V, *ojIs1*[GFP:TBB-2], *xsIs3*[HIS-11:GFP], and *ltIs25* [pAZ132; *pie-1*/GFP::*tba-2*; *unc-119* (+)]. Some nematode strains were provided by the Caenorhabditis Genetics Center, which is funded by the National Institutes of Health (NIH) National Center for Research Resources (NCRR).

RNA Interference

RNAi was performed with the feeding method as described [44], with double feeding vectors where indicated. L4 larvae were picked onto the plates and incubated at 25°C for at least 24 hr for all experiments. We ensured that RNAi depletion resulted in fully penetrant phenotypes, and where possible, we reproduced the phenotypes with well-characterized alleles.

Immunolocalization

To simultaneously visualize serine-19-phosphorylated rMLC and F-actin, we removed the eggshell as described [45] and fixed for 25 min in 4% formaldehyde, 0.2% glutaraldehyde, 0.1 mg/ml lysolecithin (Sigma), 60 mM Pipes, 25 mM HEPES, 10 mM ethylene glycol tetraacetic acid (EGTA), 2 mM $MgCl_2$, and 100 mM dextrose. The embryos were blocked in 5% goat serum, 1% bovine serum albumin for 30 min, and then sequentially stained with rabbit anti-phosphomyosin regulatory light chain 2 (ser-19) at 1:200 (Cell Signaling Technology) followed by a mixture of Alexa-568 anti-rabbit IgG at 1:600 (Molecular Probes) and Alexa-488-conjugated phallicidin (1 unit/100 μl; Molecular Probes). DNA was stained with 1 μg/ml DAPI. Embryos were mounted in fluoromount G (Southern Biotechnology) and cured overnight at room temperature (RT) before images were collected. These images were collected on a BioRad radiance confocal microscope.

Microscopy

Images were acquired with a 63×/1.4 numerical aperture (NA) objective on a Zeiss Axiovert 200M equipped with a Yokogawa CSU-10 spinning-disk unit (McBain), illuminated with a 50mW 473 nm laser (Cobolt). Images were captured on a Cascade 512B EM-CCD camera (Photometrics) with MetaMorph (Molecular Devices). For the imaging of cortical NMY-2:GFP, five cortical planes were acquired covering a z distance of 3 μm. Z series were acquired every 2.5 s for a high temporal resolution. To simultaneously image NMY-2:GFP and HIS:GFP or NMY-2:GFP and TUB:GFP with a high time resolution, every 3 s, we acquired five cortical planes covering a z distance of 3 μm and a single plane in the center of the embryo. To quantify chromosome condensation in embryos expressing NMY-2GFP and HIS:GFP, we acquired two stacks of five planes spanning either 3 μm on the cortex or 5 μm in the center of the embryo every 10 s. The Z stacks were projected with a maximum-intensity algorithm, and the resulting images were assembled into a movie. For the imaging of microtubules and myosin with high spatial resolution, Z stacks of 30 planes spaced by 0.5 μm were acquired from embryos expressing both TUB:GFP and NMY-2:GFP. The Z stack was then converted into 8 bit TIFFs with Metamorph and visualized with OsiriX (http://homepage.mac.com/rossetantoine/osirix/). Kymographs were assembled from maximum pixel intensities over three pixels on central linescan along the A/P axis of the embryo. All imaging was performed with a stage temperature of 24°C –25°C; all temperature-sensitive alleles exhibited full penetrance under these conditions (n > 30 embryos for each allele).

Data Analysis

For analyzing the distribution of cortical myosin, five cortical planes spanning a z distance of 3 μm were acquired every 2.5 s. The Z stacks were projected with a maximum intensity projection. Eight time points (20 s) directly after anaphase onset were selected by the appearance of cortical myosin foci and projected again with maximum projection to accumulate foci over time. Intensity values of pixels perpendicular to the A/P axis were averaged with ImageJ, and the measurements were binned into 50 regions along the A/P axis to allow comparison between embryos of variable length. Average values for at least eight individual recordings were plotted. For determining the total cortical intensities, the same projected images were used to determine the average intensities per pixel with Metamorph. Chromosome condensation was measured as described [46].

Supplemental Data

Three figures and seven movies are available at http://www.current-biology.com/cgi/content/full/17/15/1286/DC1/.

Acknowledgments

The authors thank Erin McCarthy and Bob Goldstein for discussions concerning RPT-6, Paul Maddox for providing a GFP:tubulin-expressing strain, and Ron Rock for assistance in assembling the spinning-disk confocal microscope. The Glotzer Lab is supported by National Institute of General Medical Sciences (NIGMS) R01 GM074743. E.M. was supported by NIGMS 5P50 GM66050-05.

Received: April 18, 2007
Revised: June 21, 2007
Accepted: June 26, 2007
Published online: August 2, 2007

References

1. Glotzer, M. (2005). The molecular requirements for cytokinesis. Science *307*, 1735–1739.
2. Yuce, O., Piekny, A., and Glotzer, M. (2005). An ECT2-centralspindlin complex regulates the localization and function of RhoA. J. Cell Biol. *170*, 571–582.
3. Bement, W.M., Benink, H.A., and von Dassow, G. (2005). A microtubule-dependent zone of active RhoA during cleavage plane specification. J. Cell Biol. *170*, 91–101.
4. Piekny, A., Werner, M., and Glotzer, M. (2005). Cytokinesis: Welcome to the Rho zone. Trends Cell Biol. *15*, 651–658.
5. Raich, W.B., Moran, A.N., Rothman, J.H., and Hardin, J. (1998). Cytokinesis and midzone microtubule organization in Caenorhabditis elegans require the kinesin-like protein ZEN-4. Mol. Biol. Cell *9*, 2037–2049.
6. Powers, J., Bossinger, O., Rose, D., Strome, S., and Saxton, W. (1998). A nematode kinesin required for cleavage furrow advancement. Curr. Biol. *8*, 1133–1136.
7. Jantsch-Plunger, V., Gönczy, P., Romano, A., Schnabel, H., Hamill, D., Schnabel, R., Hyman, A.A., and Glotzer, M. (2000). CYK-4: A Rho family GTPase activating protein (GAP) required for central spindle formation and cytokinesis. J. Cell Biol. *149*, 1391–1404.
8. Verbrugghe, K.J., and White, J.G. (2004). SPD-1 is required for the formation of the spindle midzone but is not essential for the completion of cytokinesis in C. elegans embryos. Curr. Biol. *14*, 1755–1760.
9. Bonaccorsi, S., Giansanti, M.G., and Gatti, M. (1998). Spindle self-organization and cytokinesis during male meiosis in asterless mutants of Drosophila melanogaster. J. Cell Biol. *142*, 751–761.
10. Dechant, R., and Glotzer, M. (2003). Centrosome separation and central spindle assembly act in redundant pathways that regulate microtubule density and trigger cleavage furrow formation. Dev. Cell *4*, 333–344.
11. Bringmann, H., and Hyman, A.A. (2005). A cytokinesis furrow is positioned by two consecutive signals. Nature *436*, 731–734.
12. Canman, J.C., Cameron, L.A., Maddox, P.S., Straight, A., Tirnauer, J.S., Mitchison, T.J., Fang, G., Kapoor, T.M., and Salmon, E.D. (2003). Determining the position of the cell division plane. Nature *424*, 1074–1078.
13. Kurz, T., Pintard, L., Willis, J.H., Hamill, D.R., Gonczy, P., Peter, M., and Bowerman, B. (2002). Cytoskeletal regulation by the Nedd8 ubiquitin-like protein modification pathway. Science *295*, 1294–1298.
14. Canman, J.C., Hoffman, D.B., and Salmon, E.D. (2000). The role of pre- and post-anaphase microtubules in the cytokinesis phase of the cell cycle. Curr. Biol. *10*, 611–614.
15. Nishimura, Y., and Yonemura, S. (2006). Centralspindlin regulates ECT2 and RhoA accumulation at the equatorial cortex during cytokinesis. J. Cell Sci. *119*, 104–114.
16. Somers, W.G., and Saint, R. (2003). A RhoGEF and Rho family GTPase-activating protein complex links the contractile ring to cortical microtubules at the onset of cytokinesis. Dev. Cell *4*, 29–39.
17. Bringmann, H., Cowan, C.R., Kong, J., and Hyman, A.A. (2007). LET-99, GOA-1/GPA-16, and GPR-1/2 are required for aster-positioned cytokinesis. Curr. Biol. *17*, 185–191.
18. Munro, E., Nance, J., and Priess, J.R. (2004). Cortical flows powered by asymmetrical contraction transport PAR proteins to establish and maintain anterior-posterior polarity in the early C. elegans embryo. Dev. Cell *7*, 413–424.
19. Gonczy, P., Echeverri, C., Oegema, K., Coulson, A., Jones, S.J., Copley, R.R., Duperon, J., Oegema, J., Brehm, M., Cassin, E., et al. (2000). Functional genomic analysis of cell division in C. elegans using RNAi of genes on chromosome III. Nature *408*, 331–336.
20. Schonegg, S., and Hyman, A.A. (2006). CDC-42 and RHO-1 coordinate acto-myosin contractility and PAR protein localization during polarity establishment in C. elegans embryos. Development *133*, 3507–3516.
21. Motegi, F., Velarde, N.V., Piano, F., and Sugimoto, A. (2006). Two phases of astral microtubule activity during cytokinesis in C. elegans embryos. Dev. Cell *10*, 509–520.
22. Prokopenko, S.N., Brumby, A., O'Keefe, L., Prior, L., He, Y., Saint, R., and Bellen, H.J. (1999). A putative exchange factor for Rho1 GTPase is required for initiation of cytokinesis in Drosophila. Genes Dev. *13*, 2301–2314.
23. Hird, S.N., and White, J.G. (1993). Cortical and cytoplasmic flow polarity in early embryonic cells of Caenorhabditis elegans. J. Cell Biol. *121*, 1343–1355.
24. Severson, A.F., Baillie, D.L., and Bowerman, B. (2002). A Formin Homology protein and a profilin are required for cytokinesis and Arp2/3-independent assembly of cortical microfilaments in C. elegans. Curr. Biol. *12*, 2066–2075.
25. Severson, A.F., Hamill, D.R., Carter, J.C., Schumacher, J., and Bowerman, B. (2000). The aurora-related kinase AIR-2 recruits ZEN-4/CeMKLP1 to the mitotic spindle at metaphase and is required for cytokinesis. Curr. Biol. *10*, 1162–1171.
26. Hannak, E., Kirkham, M., Hyman, A.A., and Oegema, K. (2001). Aurora-A kinase is required for centrosome maturation in Caenorhabditis elegans. J. Cell Biol. *155*, 1109–1116.
27. Hachet, V., Canard, C., and Gonczy, P. (2007). Centrosomes promote timely mitotic entry in C. elegans embryos. Dev. Cell *12*, 531–541.
28. Portier, N., Audhya, A., Maddox, P.S., Green, R.A., Dammermann, A., Desai, A., and Oegema, K. (2007). A microtubule-independent role for centrosomes and aurora a in nuclear envelope breakdown. Dev. Cell *12*, 515–529.
29. Rappaport, R. (1961). Experiments concerning the cleavage stimulus in sand dollar eggs. J. Exp. Zool. *148*, 81–89.
30. Rappaport, R. (1985). Repeated furrow formation from a single mitotic apparatus in cylindrical sand dollar eggs. J. Exp. Zool. *234*, 167–171.
31. Wu, J.Q., Sirotkin, V., Kovar, D.R., Lord, M., Beltzner, C.C., Kuhn, J.R., and Pollard, T.D. (2006). Assembly of the cytokinetic contractile ring from a broad band of nodes in fission yeast. J. Cell Biol. *174*, 391–402.
32. Cowan, C.R., and Hyman, A.A. (2004). Centrosomes direct cell polarity independently of microtubule assembly in C. elegans embryos. Nature *431*, 92–96.

33. Sonneville, R., and Gonczy, P. (2004). Zyg-11 and cul-2 regulate progression through meiosis II and polarity establishment in C. elegans. Development *131*, 3527–3543.
34. Hannak, E., Oegema, K., Kirkham, M., Gonczy, P., Habermann, B., and Hyman, A.A. (2002). The kinetically dominant assembly pathway for centrosomal asters in Caenorhabditis elegans is gamma-tubulin dependent. J. Cell Biol. *157*, 591–602.
35. Gregoretti, I.V., Margolin, G., Alber, M.S., and Goodson, H.V. (2006). Insights into cytoskeletal behavior from computational modeling of dynamic microtubules in a cell-like environment. J. Cell Sci. *119*, 4781–4788.
36. Glotzer, M. (2004). Cleavage furrow positioning. J. Cell Biol. *164*, 347–351.
37. Kamijo, K., Ohara, N., Abe, M., Uchimura, T., Hosoya, H., Lee, J.S., and Miki, T. (2006). Dissecting the role of Rho-mediated signaling in contractile ring formation. Mol. Biol. Cell *17*, 43–55.
38. Wolpert, L. (1960). The mechanics and mechanism of cleavage. Int. Rev. Cytol. *10*, 163–216.
39. Schaar, B.T., and McConnell, S.K. (2005). Cytoskeletal coordination during neuronal migration. Proc. Natl. Acad. Sci. USA *102*, 13652–13657.
40. Bellion, A., Baudoin, J.P., Alvarez, C., Bornens, M., and Metin, C. (2005). Nucleokinesis in tangentially migrating neurons comprises two alternating phases: Forward migration of the Golgi/centrosome associated with centrosome splitting and myosin contraction at the rear. J. Neurosci. *25*, 5691–5699.
41. Enomoto, T. (1996). Microtubule disruption induces the formation of actin stress fibers and focal adhesions in cultured cells: Possible involvement of the rho signal cascade. Cell Struct. Funct. *21*, 317–326.
42. Elbaum, M., Chausovsky, A., Levy, E.T., Shtutman, M., and Bershadsky, A.D. (1999). Microtubule involvement in regulating cell contractility and adhesion-dependent signalling: A possible mechanism for polarization of cell motility. Biochem. Soc. Symp. *65*, 147–172.
43. Kaverina, I., Krylyshkina, O., Gimona, M., Beningo, K., Wang, Y.L., and Small, J.V. (2000). Enforced polarisation and locomotion of fibroblasts lacking microtubules. Curr. Biol. *10*, 739–742.
44. Timmons, L., and Fire, A. (1998). Specific interference by ingested dsRNA. Nature *395*, 854.
45. Costa, M., Draper, B.W., and Priess, J.R. (1997). The role of actin filaments in patterning the Caenorhabditis elegans cuticle. Dev. Biol. *184*, 373–384.
46. Kaitna, S., Pasierbek, P., Jantsch, M., Loidl, J., and Glotzer, M. (2002). The aurora B kinase AIR-2 regulates kinetochores during mitosis and is required for separation of homologous Chromosomes during meiosis. Curr. Biol. *12*, 798–812.